A&A 411, L243–L251 (2003)
DOI: 10.1051/0004-6361:20031363

Astronomy & Astrophysics

JEM–X inflight performance⋆

S. Brandt[1], C. Budtz-Jørgensen[1], N. Lund[1], N. J. Westergaard[1], I. L. Rasmussen[1], K. H. Andersen[1], J. Chenevez[1], A. Hornstrup[1], P. A. Jensen[1], S. Laursen[1], K. Omø[1], C. A. Oxborrow[1], S. M. Pedersen[1], J. Polny[1], H. Andersson[2], T. Andersson[2], O. Vilhu[3], J. Huovelin[3], S. Maisala[3], M. Morawski[4], G. Juchnikowski[4], E. Costa[5], M. Feroci[5], A. Rubini[5], M. Rapisarda[6], E. Morelli[7], F. Frontera[8], C. Pelliciari[8], G. Loffredo[8], V. Carassiti[8], V. Reglero[9], S. Martínez Núñez[9], S. Larsson[10], R. Svensson⋆⋆,[10], A. A. Zdziarski[11], A. Castro-Tirado[12], M. Goria[13], G. Giulianelli[13], M. Rezazad[14], F. Cordero[14], M. Schmidt[14], R. Carli[15], P. L. Jensen[15], G. Sarri[15], C. Gomez[15], A. Orr[15], R. Much[15], H. W. Schnopper[16], and P. Kretschmar[17,18]

[1] Danish Space Research Institute, Juliane Maries Vej 30, 2100 Copenhagen Ø, Denmark
[2] Metorex International Oy, Nihtisillankuja 5, PO Box 85, 02631 Espoo, Finland
[3] Observatory, PO Box 14, 00014, University of Helsinki, Finland
[4] Space Research Center, Bartycka 18A 00-716, Warsaw, Poland
[5] Instituto de Astrofisica CNR, via del Fosso del Cavaliere 100, 00133 Rome, Italy
[6] ENEA-Frascati UTS-Fusione, via Enrico Fermi 45, 00045 Frascati, Italy
[7] IASF-Bologna, via Gobetti 101, 40129, Bologna, Italy
[8] Dipartimento di Fisica, University of Ferrara, via del Paradiso 12, 44100 Ferrara, Italy
[9] GACE, University of Valencia, PO Box 20085, 46071 Valencia, Spain
[10] Stockholm University, Roslagstullgatan 21, Stockholm, Sweden
[11] Copernicus Astronomical Center, Bartycka 18, 00-716, Warsaw, Poland
[12] Instituto de Astrofísica de Andalucía (IAA-CSIC), PO Box 03004, 18080 Granada, Spain
[13] Alenia Spazio, Space Division, Corso Marche 41, 10146 Torino, Italy
[14] ESOC, Robert-Bosch Str. 5, 64293 Darmstadt, Germany
[15] ESTEC, Keplerlaan 1, Postbus 299, 2200 AG Noordwijk, The Netherlands
[16] Harvard-Smithsonian Center for Astrophysics, 60 Garden Street, Cambridge, MA 02138, USA
[17] Max-Planck-Institut für Extraterrestrische Physik Gießenbachstr., 85748 Garching, Germany
[18] INTEGRAL Science Data Center, Chemin d'Écogia 16, Versoix, Switzerland

Received 15 July 2003 / Accepted 4 September 2003

Abstract. We summarize the inflight performance of JEM–X, the X–ray monitor on the INTEGRAL mission during the initial ten months of operations. The JEM–X instruments have now been tuned to stable operational conditions. The performance is found to be close to the pre-launch expectations. The ground calibrations and the inflight calibration data permit to determine the instruments characteristics to fully support the scientific data analysis.

Key words. instrumentation: detectors – X–rays: general

1. Introduction

Two JEM–X coded mask telescopes (Lund et al. 2003; Budtz-Jørgensen et al. 2003; Schnopper et al. 1996; Westergaard et al. 1997; Budtz-Jørgensen et al. 1997) constitute the X–ray monitor on the INTEGRAL mission (Winkler et al. 2003). The JEM–X instruments have now been tuned to stable operational conditions. Although some settings differ from what was originally planned, the actual performance is close to the pre-launch expectations.

The ground calibrations (Loffredo et al. 2003) and the inflight calibration data, primarily those from the observations of the Crab in February 2003, are of exellent quality and permits to determine the instruments characteristics adequately for the support of the scientific analysis.

The flight configuration was achieved during the first two months of commissioning. However, the fine tuning of parameters, partly as a result of long term performance trends, is still ongoing.

A set of tools for the analysis of the JEM–X data is publicly available from the INTEGRAL Science Data Center (ISDC)

Send offprint requests to: S. Brandt, e-mail: sb@dsri.dk

⋆ Based on observations with INTEGRAL, an ESA project with instruments and science data centre funded by ESA member states (especially the PI countries: Denmark, France, Germany, Italy, Switzerland, Spain), Czech Republic and Poland, and with the participation of Russia and the USA.

⋆⋆ Deceased.

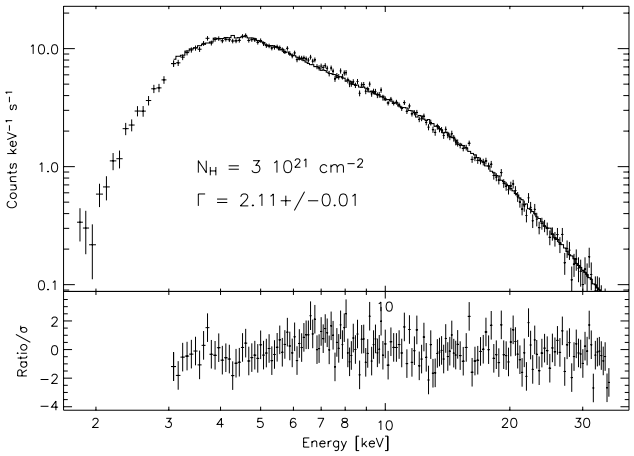

Fig. 1. The Crab spectrum as measured in JEM–X2 with an integration time of 2000 s. The spectrum has been fitted in XSPEC with a powerlaw and an absorption of 3×10^{21} cm^{-2} (frozen). The fit is for energies above 3 keV. Below this limit the response is not very well determined.

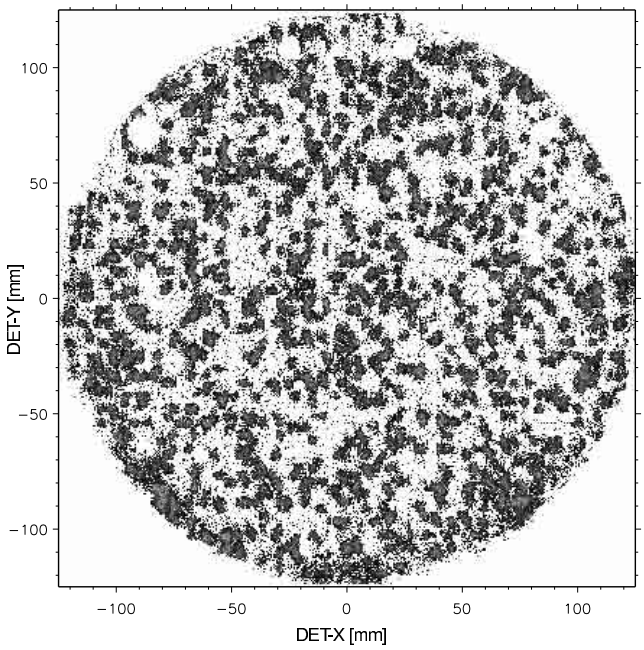

Fig. 2. The shadowgram of Cyg X-1 (on-axis) in JEM–X1 in energy range 3–35 keV. The detector coordinates, (DETX, DETY), are given in mm.

(Courvosier et al. 2003; Westergaard et al. 2003). The JEM–X software team is constantly working to improve and refine these tools.

2. JEM–X scientific performance

2.1. Energy range and resolution

The detector energy resolution is primarily determined by the number of free electrons liberated during the X–ray absorbtion process, and the relative energy resolution derived from the ground calibrations was:

$$\frac{\Delta E_{\rm fwhm}}{E} = 0.40 \times \sqrt{\frac{1}{E\,[\rm keV]}}. \quad (1)$$

In space the effective energy resolution is derived from the internal calibration sources and the xenon K_α fluorescence lines, which are detected all over the sensitive area as part of the general background. It is found that the energy resolution has an additional "noise" term, and has the following empiric functional form:

$$\frac{\Delta E_{\rm fwhm}}{E} = 0.40 \times \sqrt{\frac{1}{E\,[\rm keV]} + \frac{1}{60}}. \quad (2)$$

We believe that the added noise is induced by cosmic rays, causing local temporal gain variations. This is supported by the observed episodes of jitter in the gain in the local areas of the four internal calibration sources (see also Sect. 3.2). The energy resolution of the 22 and 25 keV lines of the internal calibration sources is better than 10% in both JEM–X1 and JEM–X2. The spatial gain variations over the microstrip plate are at the level of ±10%. The details of these spatial variations have changed somewhat since the ground calibrations as a consequence of a lower gain setting used in space, and possibly also by the radiation environment in space. We are optimizing these corrections using the xenon K_α fluorescence lines.

The low energy thresholds of the detectors have been slightly modified by the decrease of the detector gain, described in Sect. 3.1. Analysis show that the 50% efficiency level is reached at 4.2 keV instead of at 3.5 keV in the ground calibrations. However, the performed observations of Sco X–1 clearly show that meaningful observations can still be made down to 3 keV.

The upper energy limit of JEM–X has not been affected by the change in gas gain, as this limit is determined by the gradually diminishing absorbtion cross section of the xenon gas above 25 keV. In order to reduce the telemetry usage we apply an upper level signal cut-off around 40 keV. An example of the raw count rate spectrum of the Crab is shown in Fig. 1.

The significant spatial gain variation of the detector has implications for the resolution of the energy spectra. In turn, this determines the recommended choice of telemetry formats. Only for data in the "full imaging" format, where time, pulse-height, and postion of each event is transmitted, can the full spectral resolution be achieved on ground.

2.2. Photon localization

The starting point for the JEM–X imaging analysis is the "shadowgram", the sky projected onto the detector through the coded mask. Figure 2 shows such a "shadowgram" obtained from an on-axis observation of Cyg X-1 in the energy band from 3 to 35 keV. Figure 3 displays the corresponding telescope 2D Point Spread Function (PSF). The detector coordinates are given in mm, where 1 mm in the detector plane closely corresponds to 1′ on the sky. The PSF is well represented by a 2D Gaussian function with standard deviations of $\sigma_x = \sigma_y = 1.45$ mm, corresponding to a full-width-half-maximum (FWHM) of 3.4′. This width agrees well with the nominal geometric resolution

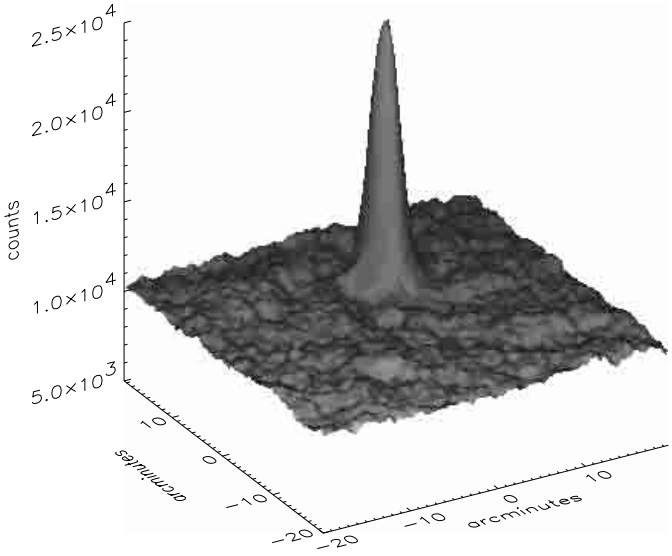

Fig. 3. Derived point spread function of Cyg X-1 (on-axis) in JEM–X1 from data of the shadowgram shown in Fig. 2. The plot shows a $50' \times 50'$ section of the field of view.

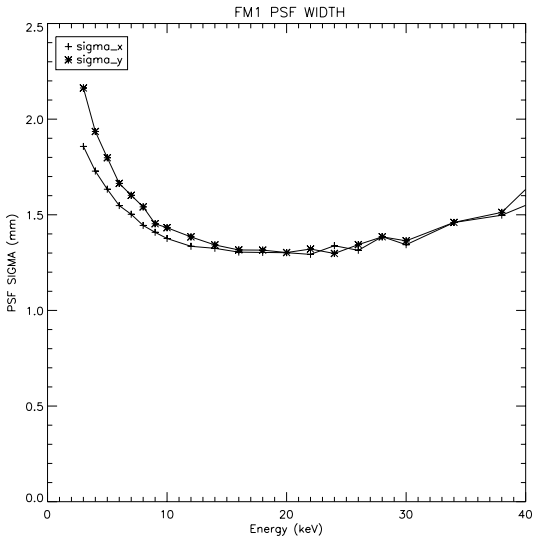

Fig. 4. The width (shown as standard deviation) of the Point Spread Function (PSF) as a function of energy.

of 3.35′ determined my the mask pixel size (Lund et al. 2003). The JEM–X PSF was analyzed as a function of X–ray energy. The energy dependence of the width of the PSF is shown in Fig. 4. The increase of the width towards lower energies reflects the decrease of the detector position resolution (see Fig. 5) as the signal-to-electronic noise ratio for each detected X–ray photon decreases. The spatial resolution of the detector is sufficient to achieve useful PSFs across the full 3–35 keV band. We notice that an optimal data analysis must take the energy dependence of the PSF into account.

2.3. Timing stability and resolution

The extended observations of the Crab pulsar have permitted an end-to-end test of the timing properties of the JEM–X data,

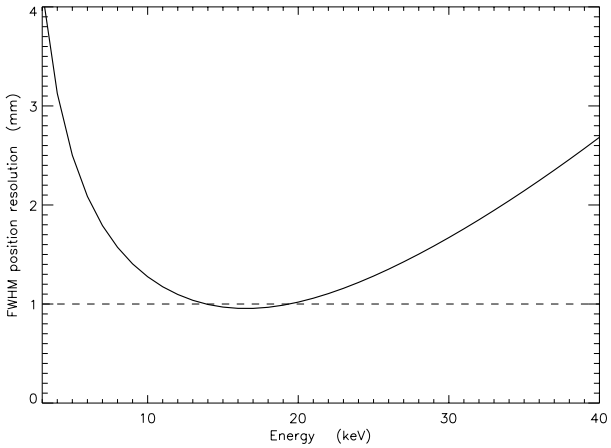

Fig. 5. The intrinsic position resolution of the JEM–X detector (FWHM). The positions are rounded to 1 mm accuracy in the telemetry, as indicated by the dashed line.

and the results are reported in detail elsewhere in this volume (Brandt et al. 2003). Observations separated by 20 days were used to determine the absolute timing of the arrival of the main Crab pulse. The absolute timing accuracy was found to be better than 100 μs, and demonstrated a clock stability of the combined system of the JEM–X clock, the INTEGRAL onboard clock, and the ground segment better than 10^{-9}. The JEM–X time stamps have a resolution of 122 μs. However, as the analysis shows, the phase of the timing bins is determined with a much better accuracy, consistent with the on-ground timing test results showing that the bin phase is accurate to within a few μs (Timm et al. 2001; Lund 2002).

2.4. Source positioning uncertainty

The determination of the sky-position of a source consists of two parts: Instrument boresight with respect to star-tracker direction, and the intrinsic instrument position determination. The Cyg X-1 observations early in the mission were used for an initial determination of the misalignment matrix. The intrinsic position determination is based on the corrected detector positions of the events. A study of the source position accuracy obtained with the JEM–X standard software at ISDC (Westergaard et al. 2003) has been made from the Crab calibration observations and the result is shown in Fig. 6. The systematic deviation of 25″ should be reduced by improving the misalignment matrix.

When the Crab is observed away from the pointing axis the position accuracy drops because of a weaker signal to noise ratio and the parallax effect, which causes a smearing of the detector image due to X–rays interacting at varying depths in the detector gas volume. Figure 7 shows the position accuracy as a function of off-axis angle. Improvements of the imaging software will probably reduce the scatter. Analysis also show intrinsic systematic errors corresponding to different positions within the field-of-view. For sources lying less than 4° off-axis the systematics are less than 10″. Between 4 and 5° the systematic errors are more difficult to determine because of the

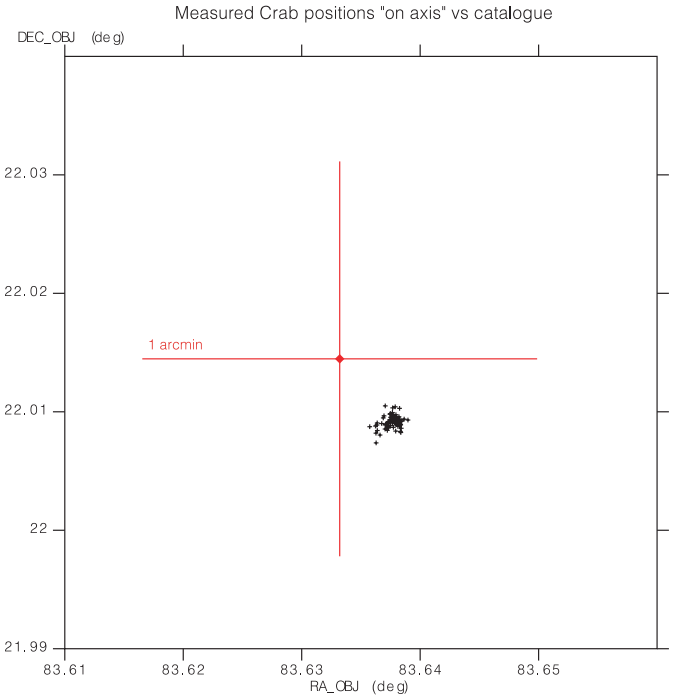

Fig. 6. Distribution of the Crab position from pointings where it is found close to the pointing axis, using the misalignment matrix implemented in the first version of the ISDC software. The large cross is centered on the catalog position for the Crab Pulsar, but the centroid of combined Nebula and Pulsar emission is found to be displaced by ≈6″ to the NW (upper left).

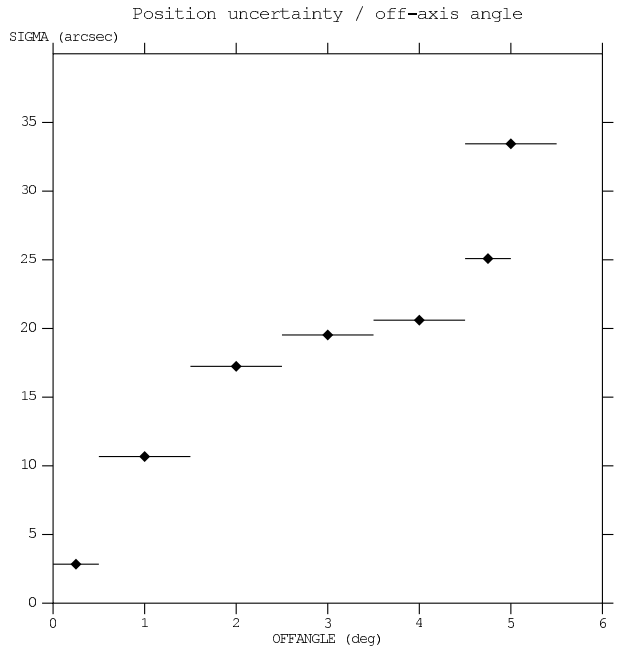

Fig. 7. The Crab position scatter (σ), in units of arc-seconds, as a function of off-axis angle in degrees. This scatter in relative position determination represents the absolute positioning capability of JEM–X, once systematic are fully understood.

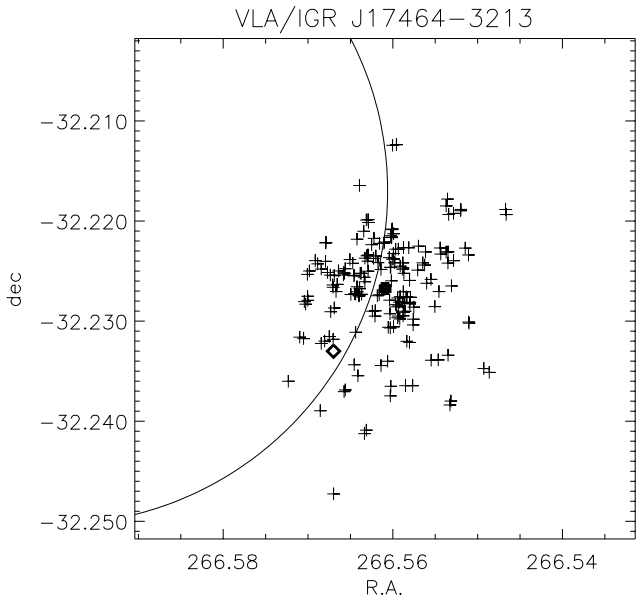

Fig. 8. JEM–X localizations of the INTEGRAL source IGR J17464-3213. The circle segment is part of the original IBIS error circle, the diamond is the suggested radio counterpart, and the bold cross is the centroid of the JEM–X localizations. The JEM–X misalignment matrix is not yet final, so the discrepancy between the radio position and the JEM–X position is not significant.

rapidly falling efficiency of the instrument, but they appear to increase to about 20′ at 5°. Some of this effect is due to parallax effects and these may be compensated for in the analysis. Beyond 5° off-axis we do not recommend to use JEM–X for source positioning.

An example of the position capability is the detection of the INTEGRAL source IGR J17464-3213, which was discovered by IBIS (Revnivtsev et al. 2003). Figure 8 shows the clustering of 183 independent JEM–X detections of this source around a position near the radio position determined by the VLA (Rupen et al. 2003). These data are the result of an off-line analysis for which the instrument misaligment matrix clearly also needs some additional fine tuning. The centroid of the JEM–X position is about 25′ from the VLA position, and the RMS scatter of the JEM–X positions is 14′.

The Crab observations also provided an opportunity to demonstrate the stability and the statistical precision of the source location with JEM–X at the level of 1′. It is known from several X–ray imaging studies of the Crab complex (Pelling et al. 1987) that the pulsar is offset in position by 10′–20′ from the centroid of the nebular emission. We have made multiple position determinations for the total Crab signal, resolved according to the pulsar phase. The derived position oscillates in phase with the pulsar signal with an amplitude of ≈6′. In this situation the systematic errors cancel out, and it is possible to demonstrate that the achievable position accuracy is close to the statistical limit (for details, see Brandt et al. 2003), confirming the excellent JEM–X source location accuracy potential once systematics are properly understood.

2.5. Background

The JEM–X background has been derived from a number of empty field observations. The observed in-flight background count rates are listed in Table 1. The count rate data for the Crab (pulsar + nebula) are also shown for reference. The

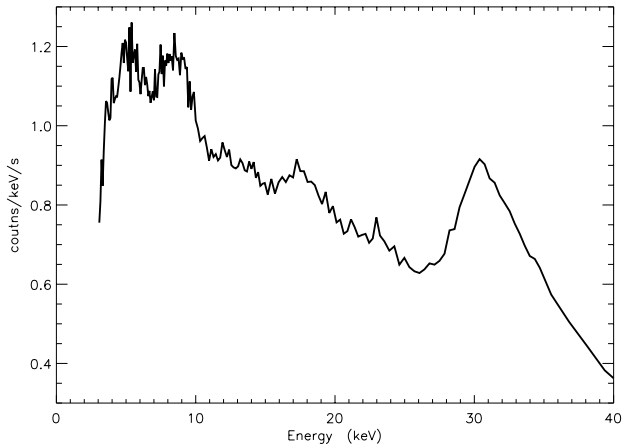

Fig. 9. Example of an empty field background spectrum measured with JEM–X2 in June 2003.

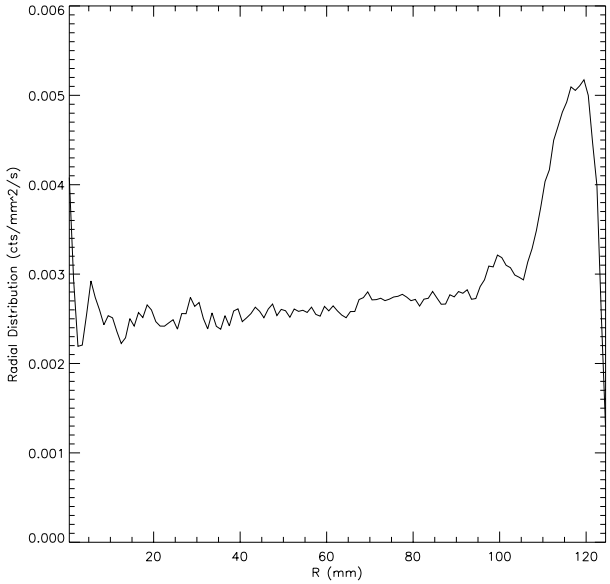

Fig. 10. The background (in units of counts/mm^2/s) as a function of radius in the detector.

background rate is about 20 cts/s in the 4 to 35 keV range. This is about a factor two higher than predicted before launch (Feroci et al. 1999).

We have identified a couple of factors contributing to this difference. A significant uncertainty existed prior to launch in the predictions of the gamma-ray background aboard INTEGRAL. This uncertainty has affected all instruments. Secondly, the reduction in the JEM–X operational gas gain has made it more critical and difficult to adjust the on-board event selection algorithm to achieve both an acceptable efficiency for X–rays below 5 keV and a high efficiency for rejecting non-X–ray events. This adjustment process has not yet reached a final and fully satisfactory state.

We note, that with a trigger rate of ≈1500 background events per second the accepted particle induced background rate of 15 c/s, of which most are in fact X–rays, the suppression of particles and particle induced X–rays is better than 99%.

Table 1. The JEM–X actual count rates for the Crab on-axis, the diffuse X–ray background (DXB), and cosmic ray induced background (CR), and the total background in 3 different energy intervals and in the total energy range. The DXB contribution has been derived by fitting a model spectrum.

Interval (keV)	Crab counts/s	DXB counts/s	CR counts/s	Total bkg counts/s
3–10	83	3.0	3.1	6.1
10–20	27	1.8	5.1	6.9
20–35	5.4	0.5	6.5	7.0
3–35	115	5.3	14.7	20.0

Figure 9 illustrates the background energy spectra measured under these conditions. The detected background lines from Cu, Mo, Xe fluorescence and a weak uranium contamination of the beryllium window were also observed during the ground calibrations. Further details about the modeling of the JEM–X are reported by Huovelin et al. (2003).

The radial variation in the background across the detector is shown in Fig. 10. The increase of the background towards the edge of the detector is noticeable.

Presently, it is believed that the flux of hard X– and γ–rays produced by cosmic rays in the surrounding INTEGRAL spacecraft and payload elements is significantly higher than expected. The increase of the background in JEM–X towards the edge of the detector is rather natural, if this arises from photons generated in the material around the JEM–X detectors; such an increase would be more difficult to understand if the background was caused by the direct traversals of the detector volume by cosmic rays.

When the Sun is active and the satellite attitude is such that the Sun illuminates the JEM–X masks the soft X–ray background in JEM–X may temporarily increase substantially. These situations are, however, relatively rare and only a few observations are affected by this problem. It is believed that X–rays from the Sun can be scattered into the detector by the mask and its support structure.

So far there has been no indication of a significant long term increase in the background due to radiation activation of the detectors or their surroundings. The monitoring of the background orbital and pointing dependencies will continue.

2.6. Effective area and effective field-of-view

The on-axis effective area of the JEM–X detector is nominally the area of the detector window (491 cm^2), reduced by the 15% covered by the collimator footprint. Another reduction of the effective area is caused by the loss of some anode strips early in the mission (see Sect. 3.1). At present there are 42 dead anodes, out of 256, in JEM–X2 removing another 16 % of the area. A map of the JEM–X2 detector with indication of the dead anodes is shown in Fig. 11.

The uneven distribution of the background (see Fig. 10) makes it advantageous to remove a further 15% of the detector area to achieve an optimal signal to noise ratio for the data. These reductions bring the effective area of the JEM–X detectors to about 300 cm^2. The open fraction of the coded mask

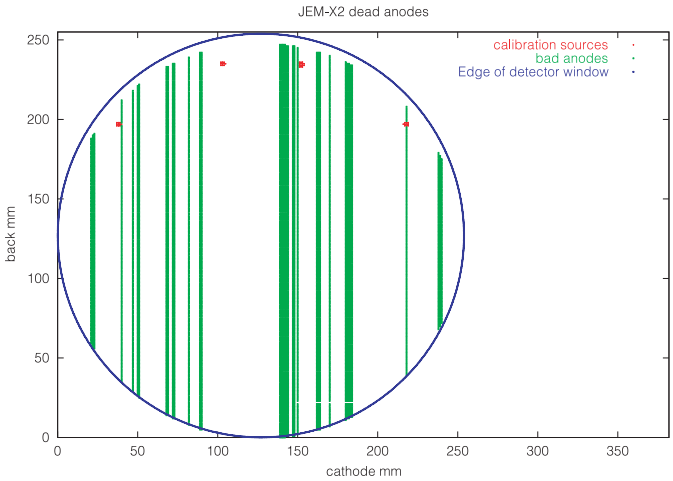

Fig. 11. Map of the JEM–X2 detector marking insensitive areas caused by dead anode strips.

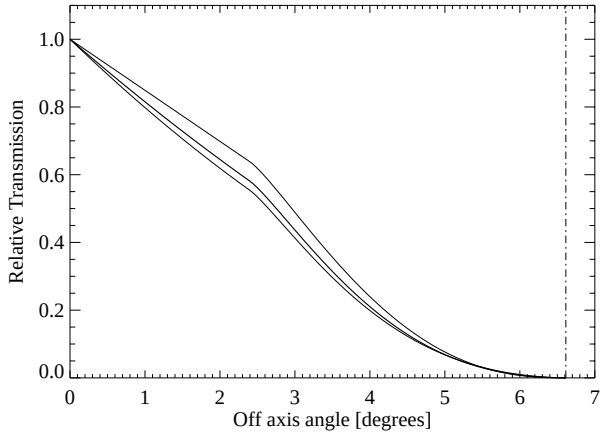

Fig. 12. The relative off-axis response of JEM-X. The thick curve shows the transmission through the collimator averaged over azimuth angles. Due to the square pattern of the collimator, an azimuthal dependence is seen. The upper curve shows the transmission along the diagonal direction and the lower curve the transmission along the walls.

was chosen at 1/4 (Lund et al. 2003), and taking the mask support structure into account the total transmission of the mask is 22%. Thus, an on-axis source will illuminate about 66 cm^2 of sensitive and useful detector area.

The collimator and the mask limit the JEM–X field of view (see Fig. 12). We have found that, although the zero transmission angle of the collimator nominally is 6.6° off axis, in practice the transmission of the collimator beyond an off axis angle of 5° is so low that only the very brightest sources can be observed at larger angles.

2.7. Deadtime

The deadtime of the JEM–X detector has been determined to be less than 12% during normal observations, without any strong sources in the field of view. For observations of stronger sources the deadtime increases by one percent for each

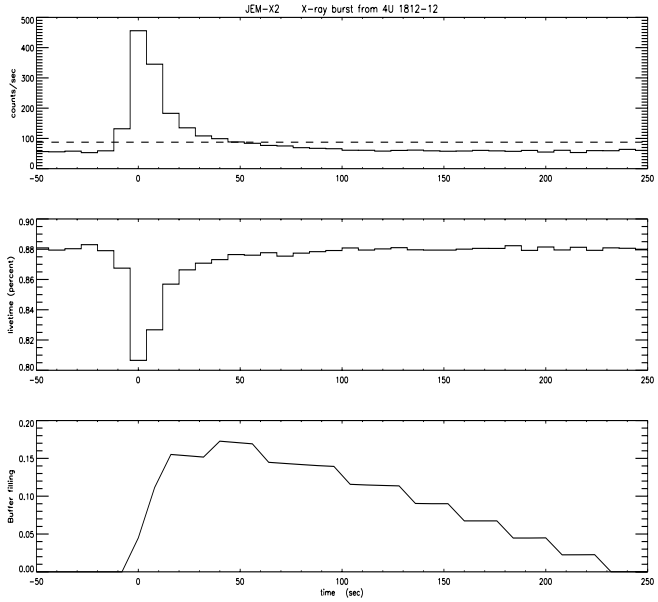

Fig. 13. The upper panel shows the detected count rate during a bright (5 Crab) X–ray burst from 4U 1812-12. The dashed line indicate the telemetry allocation. The middle panel shows the derived livetime for the detector, where we see a decrease from 88% to around 81% at the peak of the burst. The lower panel shows the filling level of the buffer holding event waiting to be transmitted to ground. The queue only reach a level less than 20% of that required before activating the grey filter mechanism.

additional 55 counts/sec in accepted X–ray events. This means that the deadtime for an observation of the Crab on-axis increases by about 2% to a total of 14%.

The deadtime is derived from the housekeeping data providing information about the number of triggers being handled in the individual branches of the onboard processing, and an example is shown in Fig. 13. Detailed knowledge about the deadtimes introduced in each channel enables the calculation of the total deadtime with an 8 s time resolution. Calculation of the deadtime with finer time resolution than 8 s, as required during short, but very intense X–ray bursts, is also possible, as the background can be considered constant and the differential deadtime is calculated from the increase in accepted events.

2.8. Source sensitivity

The source sensitivity is critically dependent on a detailed model of the detector performance, as well as an accurate background model. The first generation of imaging tools implemented for the general users at ISDC is based on the ground calibrations and certain idealized assumptions about the detector performance (Westergaard et al. 2003). This software does not yet reach the full potential of the JEM–X. Much of the science data from JEM–X2 have been analyzed with off-line imaging tools in preparation for the next generation of image analysis software. The achieved source detection sensitivity is outlined in Fig. 14. For a typical individual INTEGRAL pointing (“science window”) of 2000 s duration the 5σ detection level is reached by a 5 mCrab source on-axis. Further

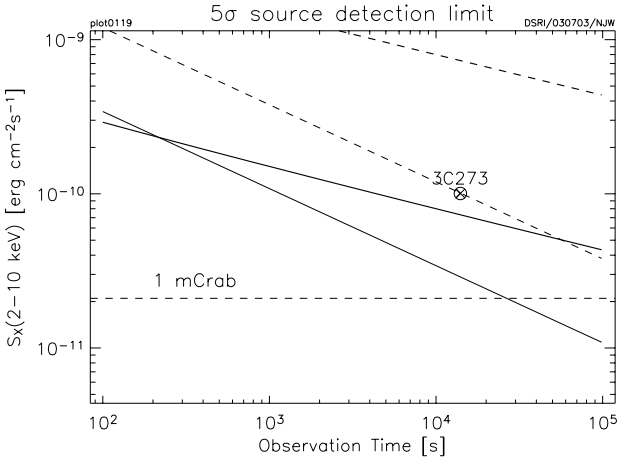

Fig. 14. 5σ source detection limit as a function of exposure time for a single JEM–X unit for an on-axis source. The lower thin solid curve has been calculated disregarding the imaging capability. The thick solid curve represents the detection limit in the deconvolved image. In both cases no other sources are assumed present in the FOV. When there is a total of 1 Crab extra sources then the dashed lines apply. The source strength is given in the interval 2–10 keV, but the 3–20 keV flux has been used for the detection limit. An actual 10σ detection of 3C 273 at 5 mCrab in 14 ks has been overplotted.

improvements are expected, as the understanding of the instrument details and background improves.

The sensitivity shown in Fig. 14 is for an on-axis source. Most INTEGRAL observations are performed using a "dither" pattern, with pointings separated by 2°, either using 7 points in a hexagonal pattern or 25 points in a square, 5×5 pattern. With the hexagonal pattern the central source is continously within the field of view of JEM–X, and the overall signal-to-noise ratio is on average maintained at 70%, compared to an on-axis "staring" observation. The much used 5×5 pattern provides a rather poor utilization of JEM–X for point source observations. Only the inner 9 out of the 25 pointings are useful for the analysis of the central source. The overall signal to noise ratio is reduced to about 35%, and it is not possible to derive a continous light curve.

3. JEM–X engineering performance

The JEM–X engineering performance is nominal, except for the micro-strip erosion experienced in the early part of the mission and a long term gain increase discussed below.

The thermal environment is stable. The detector temperature varies with a few degrees, depending on the orientation of the spacecraft. The detector gain increases by about one percent per degree of increase of the detector temperature. This effect is similar to what was observed during ground testing.

3.1. JEM–X micro-strip performance in space

The JEM–X detectors were activated about a week after the launch of INTEGRAL. The detectors were operated at the nominal gas gain of 1500. Initially all detector systems operated and behaved as expected. However, after a few days it became apparent that the microstrip anodes eroded with an alarming rate of one anode strip, out of 256, per day.

The occurrence of the anode strip damage was not correlated with the entry into the radiation belts, and it is concluded not to be caused by protons. Rather it is suspected that cosmic ray heavy ions can initiate electrical breakdowns close to the root of the anode strips (Lund et al. 2003). Similar problems have been experienced with detectors used in ground-based accellerator experiments, where high energy nuclear collisions may produce local ionization densities similar to those occuring during cosmic ray bombardment (Hott 1998).

Apparently, the radiation tests conducted prior to launch (Budtz-Jørgensen 2000) did not fully reflect the conditions in space, where the detector is traversed by approximately one Fe-group cosmic ray nucleus per second. It appears that, at a gain of 1500, about one iron nucleus out of 10^5 can initiate a disruptive breakdown. Geometry may be a significant parameter, and we note that the "root-regions" of the anode strips occupy less than 1% of the detector area. Other factors may be the geometry of the cosmic ray track relative to the micro-strip plane, and the effects of the energy of each nucleus on its specific ionization rate.

To reduce the damage rate, the gas gain for both detectors was lowered by a factor of 3. In the "cosmic ray picture" described above, it would now take a nucleus of $Z \gtrsim 40$ to cause damage corresponding to an iron nucleus at a gain of 1500. If Fe nuclei are then no longer posing a serious danger, we have reduced the flux of potentially damaging cosmic rays by several orders of magnitude, as elements beyond the Fe-group are very rare.

The gain reduction diminished the damage rate to less than one anode strip per month. The status at the time of writing (August 2003) is that during a total of 11 months of operation at the lower gain (2 months for JEM–X1 and 9 months for JEM–X2) we have lost 6 anodes. No anodes have been lost during the past 3 months of operation. At this rate of loss the survival of the instruments should be assured for a five year period. The status of the loss of anode strips in JEM–X2 is shown in Fig. 11. As a conservative measure the observations are executed with only one detector (JEM–X2) activated.

The necessary gain reduction has affected the JEM–X performance to some degree, as discussed in Sect. 2, mainly because of the resulting decrease of the signal-to-noise ratio in the detector electronics.

3.2. Temporal gain variations

During ground calibrations it was found that the gain of JEM–X just after high voltage activation was significantly higher than nominal, and settling exponentially with a time constant of 1–2 hours. This has prompted the activation at the beginning of each orbit to be performed in two steps. Initially the high voltage is set lower than the nominal value to reduce the gain by 2/3, before proceeding to the nominal setting (see Fig. 15). This variable gain is corrected by the ground software. It has been found that both the amplitude and time constant of this

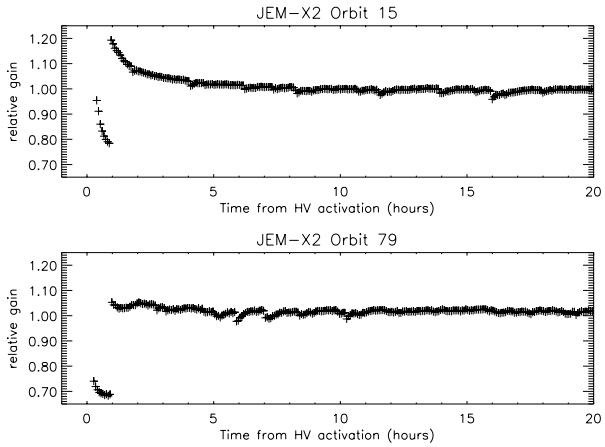

Fig. 15. The relative gain of JEM–X2 as a function of time from high voltage activation for an orbit relatively early in the mission (upper panel) and an orbit more than half a year later (lower panel). For each orbit the gain is normalized to the stable level after some hours. The initial points are recorded with a lower high voltage setting. Each point represents a calibration spectrum integrated for 256 s onboard. The gain overshoot is noticably reduced in the second example. Notice the dips at the level of a few percent, which are local and believed to be induced by cosmic rays.

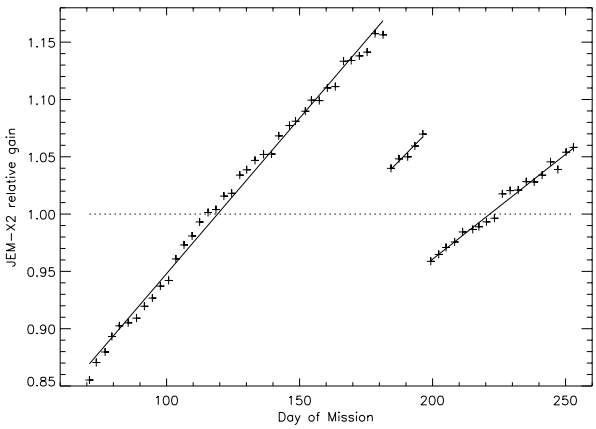

Fig. 16. The relative gain of JEM–X2 as a function of time (day of mission), normalized to the value during the Crab calibration in Feb. 2003. The plot cover the period until the end of June 2003. We initially observe a ≈1% increase per 4 days. The jumps indicate the lowering of the high voltage setting by 1 step (10 Volts), corresponding to a decrease of 12–13% in gain.

overshoot in gain at high voltage activation is reduced over time, as illustrated by the examples in Fig. 15.

Unexpectedly, the overall gain of the microstrip detectors has shown a gradual increase over time. The average gain of JEM–X2 has increased by about 1% every four days. Figure 16 shows this overall trend. After 180 days and a gain increase exceeding 25 percent it was decided to lower the high voltage setting by one step, corresponding to 10 Volts. One such further adjustment has been performed in order to keep the gain at a level comparable to the Crab calibrations. The increase continues and further high voltage adjustments are planned to keep the gain close to the reference of the Crab observations. The gain variations are tracked by the onboard calibration sources and the xenon fluorescence peak in the background and the data are corrected.

The reason for the general increase in gain and the changing profile at activation as a function of time is not fully understood, but is suspected to be related to changes of the electrical properties of the microstrip glass substrate, as it is exposed to cosmic rays (Lund et al. 2003).

4. JEM–X operations

The JEM–X operations have been smooth and the duty-cycle for the active JEM–X unit is as expected. The onboard software has performed well, and the code corrections implemented have mainly been introduced to fine tune the performance of the detector.

4.1. Radiation background

During the first months of the INTEGRAL operations it was found that the entry into the radiation belts occurred at higher altitudes than expected, sometimes at altitudes in excess of 80 000 km, compared to the pre-launch assumed altitude of 40 000 km. The INTEGRAL Radiation Monitor (IREM) is used to issue warnings to the payload against high radiation levels (Hajdas et al. 2003). It was found that JEM–X was in some cases more sensitive to the low energy electrons in the outer radiation belts than the IREM. However, the JEM–X software also has a built-in protection mechanisms to switch off the high voltages (Lund et al. 2003).

In combination with IREM, these mechanisms provide adequate protections against radiation episodes. The re-activation of the high voltage is performed manually by the Mission Operations Center (MOC) based on the IREM readings to indicate a safe radiation environment, and a minimum of useful observation time is lost.

4.2. Grey filter and telemetry requirements

The JEM–X onboard software has implemented a dynamic grey filtering logic to automatically adjust to the available telemetry allocation. In case the grey filtering is not sufficient to lower the data rate, an automatic switch to a secondary, more efficient, data format may occur (Lund 2002; Orr 2003).

The grey filter is activated when the memory containing accepted events waiting to be transmitted to ground is more than half filled. The grey filter randomly rejects a fraction of all triggers before the entry into any further event analysis. This technique minimizes the potential effects on timing analysis and allows JEM–X to operate smoothly and without gaps in the collected lightcurves at any assigned telemetry allocation. The onboard buffer allows 30 000 events in queue for transmission before activating the grey filter, so flares or bursts are normally not affected by changes in the grey filter. See Fig. 13 and also the observations of GRS 1915+105 in a higly variable state (Hannikainen et al. 2003). The queue is flushed at the start of each new pointing. The initial part of any pointing is therefore

never affected by grey filtering. The grey filter logic has proven to work well under all conditions.

The current telemetry allocation for JEM–X is allowing for JEM–X2 to transmit an average of 90 counts/sec in the preferred "full imaging" format. This allocation seems adequate for most observations. Only housekeeping data are transmitted from the dormant JEM–X1.

4.3. Operations with two JEM–X units?

Due to the concerns about the anode erosion early in the mission, at present only JEM–X2 is active. JEM–X1 is dormant; all electronics are on, but the detector high voltage is switched off. JEM–X1 has been kept in the dormant state since the commissioning phase, although it was temporarily revived during the Crab calibrations. JEM–X1 is therefore calibrated and ready to start observations.

Operating with two JEM–X units in parallel, will be a great help when detecting and verifying transients and bursts. The masks of the two units are oriented differently and artefacts in the derived images are therefore normally not overlapping. Operating with two JEM–X units will also help to recover the loss in sensitivity from which JEM–X currently suffer.

The rate of anode loss is so low that the integrated exposure operating with two JEM–X units in parallel significantly exceeds the exposure obtainable with sequential operation – even for a mission extending well beyond 5 years. The sensitivity evolution can be monitored along the way and decisions about modifications to the operations plan can be made as the mission progresses.

5. Conclusions

The commissioning and performance verification of the two JEM–X instruments on INTEGRAL has been carried out. The operability was verified and the spectral and spatial resolution has been found to be consistent with values given prior to launch. The source localization capabilities actually significantly exceed the specification values.

The sensitivity of the microstrip detectors to the space environment (specifically to the heavy nuclei in the cosmic radiation) initially threatened to limit the lifetime of the instruments.This problem has been solved by lowering the operational voltage and working at a lower gas gain. At the reduced gas gain the lower bound of our energy has moved up slightly from 3.5 to 4.2 keV.

One JEM–X unit (JEM–X1) has temporarily been placed in a dormant mode with high voltage off, until the anode erosion rate at the lower operating voltage has been safely established. At the current estimated loss rate we are confident to be able to operate JEM–X for more than 5 years, and we expect to resume operations with both JEM–X units in the fall of 2003.

The JEM–X is fully capable of fulfilling its role as the X–ray monitor on the INTEGRAL mission.

Acknowledgements. The Danish Space Research Institute acknowledges the support given to the development of the JEM–X instrument from the PRODEX programme. Authors from the University of Helsinki Observatory acknowledge the Academy of Finland, TEKES, and the Finnish space research programme Antares for financial support of this research. A. A. Zdziarski has been supported by KBN grants 5P03D00821, 2P03C00619pl,2, PBZ-054/P03/2001 and the Foundation for Polish Science. The authors from Italy acknowledge the support of Agenzia Spaziale Italia.

References

Brandt, S., Budtz-Jørgensen, C., Lund, N., et al. 2003, A&A, 411, L433

Budtz-Jørgensen, C., Westergaard, N.-J., Rasmussen, I. L., et al. 1997. In Proc. of the 2nd INTEGRAL Workshop., ed. C. Winkler, T. Courvoisier, & Ph. Durouchoux, ESA SP-382, March 1997, 651

Budtz-Jørgensen, C. 2000, HEPC Measurements at DESY, DSRI Internal Report, 10-08-2000

Budtz-Jørgensen, C., Lund, N., Westergaard, N. J., et al. 2003 JEM-X: The X–ray Monitor, in X–ray and Gamma-ray Instruments for Astronomy, ed. K. A. Flanagan, & O. H. W. Siegmund, Proc. SPIE 5165, to be published

Courvoisier, T., Walter, R., Beckmann, V., et al. 2003, A&A, 411, L53

Feroci, M., Rapisarda, M., Costa, E., et al. 1999, Astro. Lett. Comm., 39, 421

Hajdas, W., Bühler, P., Eggel, C., et al. 2003, A&A, 411, L43

Hannikainen, D. C., Vilhu, O., Rodriguez, J., et al. 2003, A&A, 411, L415

Hott, T. 1998, Nucl. Instr. and Meth., A408, 258

Huovelin, J., Maisala, S., Schultz, J., et al. 2003, A&A, 411, L253

Loffredo, G., Pelliciari, C., Frontera, F., et al. 2003, A&A, 411, L239

Lund, N., 2002, Joint European X–ray Monitor JEM–X, User Manual, Issue 5.5, October 10, 2002, `www.dsri.dk`

Lund, N., Budtz-Jørgensen, C., Westergaard, N.-J., et al. 2003, A&A, 411, L231

Orr, A. 2003, INTEGRAL Announcement of Opportunity for Observing Proposals (AO-2), JEM-X Observers Manual, ESA, INT-SOC-DOC-023, 15 July 2003

Pelling, R. M., Paciesas, W. S., Peterson, L. E., et al. 1987, ApJ, 319, 416

Revnivtsev, M., Chernyakova, M., Capitanio, F., et al. 2003, ATEL 132, `http://atel.caltech.edu`

Rupen, M. P., Mioduszewski, A. J., Dhawan, V., et al. 2003, IAU Circ., 8105

Schnopper, H. W., Budtz-Jørgensen, C., Westergaard, N. J., et al. 1996, Joint European X–ray Monitor (JEM-X): X–ray monitor for ESA's INTEGTRAL mission, in Gamma-Ray and Cosmic-Ray Detectors, Techniques, and Missions, ed. B. D. Ramsey, & T. A. Parnell, Proc. SPIE, 2806, 297

Timm, R., Carli, R., Rusticelli, S., et al. 2001, in Proc. of the 4th INTEGRAL Workshop., ed. A. Gimenez, V. Reglero, & C. Winkler, ESA SP-459, September 2001, 553

Walter, R., Favre, P., Dubath, P., et al. 2003, A&A, 411, L25

Westergaard, N.-J., Budtz-Jørgensen, C., Schnopper, H. W., et al. 1997, in Proc. of the 2nd INTEGRAL Workshop., ed. C. Winkler, T. Courvoisier, & Ph. Durouchoux, ESA SP-382, March 1997, 605

Westergaard, N. J., Kretschmar, P., Oxborrow, C. A., et al. 2003, A&A, 411, L257

Winkler, C., Courvoisier, T. J.-L., Di Cocco, G., et al. 2003, A&A, 411, L1